Monthly Notices of the ROYAL ASTRONOMICAL SOCIETY
MNRAS Advance Access published October 30, 2013
MNRAS (2013)
doi:10.1093/mnras/stt1914

Instability of the parallel electromagnetic modes in Kappa distributed plasmas – II. Electromagnetic ion–cyclotron modes

M. Lazar[1,2]★ and S. Poedts[1]★

[1]*Center for Plasma Astrophysics, Celestijnenlaan 200B, B-3001 Leuven, Belgium*
[2]*Institut für Theoretische Physik, Lehrstuhl IV: Weltraum- und Astrophysik, Ruhr-Universität Bochum, D-44780 Bochum, Germany*

Accepted 2013 October 6. Received 2013 October 4; in original form 2013 May 31

ABSTRACT

The low-frequency fluctuations of the interplanetary magnetic field are frequently attributed to electromagnetic ion–cyclotron (EMIC) waves generated either locally and self-consistently by the temperature anisotropy of ions, or in the corona and transported by the super-Alfvénic solar wind. This paper conducts a refined analysis of the EMIC instability in the presence of suprathermal populations. The anisotropic distributions are modelled with two different power-law distributions functions, the additive bi-Kappa (BK) and the more general product-bi-Kappa (PBK) distribution function. EMIC solutions are derived exactly numerically for the full range of the plasma parameters, including conditions relevant for the solar wind and magnetospheric plasmas. Accurate physical correlations are provided between the maximum growth rates and the instability threshold conditions. The expectation that the instability might be stimulated by the suprathermals is confirmed by both Kappa models, but in a complementary way: while the instability thresholds are lowered by the BK model, at higher anisotropies the growth rates are enhanced only by the PBK model.

Key words: instabilities – plasmas – waves – methods: analytical.

1 INTRODUCTION

Because collisions are rare in space plasmas, even plasmas in stationary state are out of thermal (Maxwellian) equilibrium. Energetic distributions of charged particles exhibit suprathermal tails (Pierrard & Lazar 2010; Lazar, Schlickeiser & Poedts 2012a) and anisotropies with respect to the direction of the interplanetary magnetic field (Marsch 2006). The observed deviations from thermal equilibrium are not as large as predicted by magnetic compression and adiabatic expansion, or the more energetic events triggered by the Sun. Without much influence from collisions, these deviations from thermal equilibrium are constrained by the resulting wave-instabilities, which reduce the free energy, and also scatter particles back to quasi-equilibrium (Matteini et al. 2007; Bale et al. 2009). The observed states of quasi-equilibrium are dynamically established by the exchange of energy and momentum between particles and fields.

For a rigorous description of the unstable plasma states and the resulting wave fluctuations, we need realistic models for the particle velocity distribution functions (VDFs). Empirical models are in general found by fitting with the *averaged* VDFs measured in space plasmas. In the solar wind and terrestrial magnetospheres, the family of Kappa distribution functions provides the best description for the suprathermal populations of all plasma species, including electrons (Maksimovic, Pierrard & Riley 1997), protons (Christon et al. 1991; Fisk & Gloeckler 2006) and heavier ions (Collier et al. 1996). The Kappa model is a generalized power law (Vasyliunas 1968; Tsallis 1995), which incorporates a dense and cooler core, and the more tenuous but hotter suprathermal tails. [More details may be found in recent reviews by Pierrard & Lazar (2010) and Lazar et al. (2012a).]

To describe instabilities driven by the temperature anisotropy of different plasma species, we need 3D or 2D (gyrotropic) models for the anisotropic VDFs observed in these environments. The bi-Maxwellian (BM) distribution function is frequently invoked to approach the *core* populations (e.g. at 1 au, electrons with energies up to 70 eV and protons up to a few keV) with anisotropic temperatures observed in the solar wind and terrestrial magnetosphere (Marsch 2012). To account for the effects of suprathermal *halo* populations, the anisotropic Kappa models can be introduced, either by incorporating both the core and halo populations in the same Kappa model (Collier et al. 1996; Maksimovic, Pierrard & Riley 1997; Pierrard, Maksimovic & Lemaire 1999), or by modelling the core with a Maxwellian and only the high-energy tails with a less dense but hotter power law (Thomsen et al. 1983; Maksimovic et al. 2005). The first alternative is commonly used over the second (see reviews by Hellberg, Mace & Cattaert 2005; Pierrard & Lazar 2010) on the grounds that it simplifies considerably the anisotropic model, and both the core and suprathermal populations are, in general, well fitted by the same Kappa model. A set of

★E-mail: mlazar@tp4.rub.de (ML); stefan.poedts@wis.kuleuven.be (SP)

Kappa-like anisotropic models have been proposed by Summers & Thorne (1991, see table I).

In this series of papers, starting with Lazar, Poedts & Schlickeiser (2011), hereafter called Paper I, we propose to compare the stability properties of two such anisotropic models, viz. the additive bi-Kappa (BK) and the more general product-bi-Kappa (PBK) distribution functions. These two models are described in section 2 of Paper I and in Section 2 of this paper. Trying to correlate with the observations, recent studies (Lazar et al. 2012b) associate the BK models with the slow wind, and also show that the PBK model can, at least qualitatively, reproduce the single- or double-strahl distributions observed in the fast outflows and at magnetic reconnection sites (e.g. the corotating interaction regions, where the fast wind overpasses the slow wind, and in coronal mass ejections or the top of coronal loops; Pilipp et al. 1987a; Gosling et al. 2005).

In the last two decades, the BK model has widely been used in predicting stability and dispersion properties for the anisotropic distributions with suprathermal tails, with noticeable contributions from, among others, R.M. Thorne, D. Summers, M.A. Hellberg and R.L. Mace. Some of these studies are cited in this paper, but more details can be found in the reviews by Hellberg et al. (2005) and Pierrard & Lazar (2010). Relevant for the electromagnetic ion–cyclotron (EMIC) modes is a parametric study by Xue, Thorne & Summers (1993, 1996a,b), who calculated damping and growth rates for conditions encountered in the solar wind and the Earth's magnetosphere. The PBK model has been introduced relatively recently (Basu 2008, 2009; Lazar, Schlickeiser & Poedts 2010; Paper I) based on differences between the physical mechanisms responsible for the acceleration of particles and the formation of suprathermal tails in parallel and transverse directions (also see the discussions in the Introduction of Paper I). This model is a natural generalization of the more particular Kappa–Maxwellian distribution function (the product of a 1D Kappa along the field and a Maxwellian in the perpendicular direction), proposed initially as a more realistic alternative to the BK model (Hellberg & Mace 2002; Cattaert, Hellberg & Mace 2007).

Recent studies compare these two Kappa models (Basu 2008; Basu & Grossbard 2011; Paper I), and find that dispersion properties are very sensitive to the shape of the anisotropic VDFs, leading to markedly different effects of the suprathermal populations. Thus, in Paper I we started by investigating the electron whistler–cyclotron instability, and in this paper we move our attention to lower frequencies and propose a similar comparative analysis of the EMIC instability. The observed fluctuations of the interplanetary magnetic field are frequently attributed to this instability (Nguyen, Perez & Fennell 2007; Jian et al. 2009), which is driven either locally and self-consistently by the temperature anisotropy of ions (Gary et al. 2001), or in the corona and transported by the super-Alfvénic solar wind (Isenberg 2001). For an excess of perpendicular temperature ($T_\perp > T_\parallel$), linear theory predicts a destabilization of the EMIC modes (Kennel & Petschek 1966). When the initial distribution function decreases monotonically with increasing energy, the parallel-propagating modes are the most unstable. Growth rates diminish with increasing angle to the magnetic field and vanish at some critical angle. Harder distributions with suprathermal tails will produce a larger cone of instability, but the maximum remains at parallel propagation (Kennel & Petschek 1966).

Our present analysis is, therefore, focused on the EMIC modes propagating parallel to the magnetic field. We assume an electron–proton plasma and derive in Section 3 the dispersion relations for both the PBK and BK models. The analysis of unstable solutions starts (in Section 4) with a rigorous derivation of the threshold conditions. These are then correlated with the instability growth rates, which are provided in Section 5. For the BK model, growth rates of the EMIC instability have been also derived by Xue et al. (1993). The results of the present study and the possible implications in space plasma applications are summarized in the final section (Section 6).

2 KAPPA DISTRIBUTION FUNCTIONS

For magnetized plasmas, the unperturbed velocity distributions of plasma particles can be assumed to be gyrotropic. The first model introduced in our comparative analysis is the PBK distribution function (Summers & Thorne 1991)

$$F_1(v_\parallel, v_\perp) = \frac{1}{\pi^{3/2}\theta_\perp^2\theta_\parallel}\,\frac{\Gamma[\kappa_\parallel+1]}{\kappa_\parallel^{1/2}\Gamma[\kappa_\parallel+1/2]} \times\left(1+\frac{v_\parallel^2}{\kappa_\parallel\theta_\parallel^2}\right)^{-\kappa_\parallel-1}\left(1+\frac{v_\perp^2}{\kappa_\perp\theta_\perp^2}\right)^{-\kappa_\perp-1} \tag{1}$$

in a polar coordinate system $(v_\perp\cos\phi,\, v_\perp\sin\phi,\, v_\parallel) = (v_x, v_y, v_z)$, where $\parallel$ and $\perp$ denote directions relative to the local mean magnetic field $\boldsymbol{B}_0$. This function is normalized to unity $\int \mathrm{d}^3v\, F_1 = 1$, and thermal velocities $\theta_{\parallel,\perp}$ are defined by the second-order moments of the distribution function

$$\frac{2k_BT_\parallel}{m} = v_{T_\parallel}^2 = 2\int \mathrm{d}\boldsymbol{v}\, v_\parallel^2 F_1(v_\parallel, v_\perp) = \theta_\parallel^2\,\frac{2\kappa_\parallel}{2\kappa_\parallel-1}, \tag{2}$$

$$\frac{2k_BT_\perp}{m} = v_{T_\perp}^2 = \int \mathrm{d}\boldsymbol{v}\, v_\perp^2 F_1(v_\parallel, v_\perp) = \theta_\perp^2\,\frac{\kappa_\perp}{\kappa_\perp-1}, \tag{3}$$

conditioning $\kappa_\parallel > 1/2$ and $\kappa_\perp > 1$, respectively.

The second model, extensively used in previous studies, is the additive BK distribution function

$$F_2(v_\parallel, v_\perp) = \frac{1}{\pi^{3/2}\theta_\perp^2\theta_\parallel}\,\frac{\Gamma[\kappa+1]}{\kappa^{3/2}\Gamma[\kappa-1/2]} \times\left(1+\frac{v_\parallel^2}{\kappa\theta_\parallel^2}+\frac{v_\perp^2}{\kappa\theta_\perp^2}\right)^{-\kappa-1}, \tag{4}$$

defined with a single power index $\kappa > 3/2$. The BK function is normalized to unity, $\int \mathrm{d}^3v\, F_2 = 1$, and thermal velocities $\theta_{\parallel,\perp}$ are given by

$$\frac{2k_BT_\parallel}{m} = v_{T_\parallel}^2 = 2\int \mathrm{d}\boldsymbol{v}\, v_\parallel^2 F_2(v_\parallel, v_\perp) = \theta_\parallel^2\,\frac{2\kappa}{2\kappa-3} \tag{5}$$

$$\frac{2k_BT_\perp}{m} = v_{T_\perp}^2 = \int \mathrm{d}\boldsymbol{v}\, v_\perp^2 F_2(v_\parallel, v_\perp) = \theta_\perp^2\,\frac{2\kappa}{2\kappa-3}. \tag{6}$$

The equivalent Maxwellian-like thermal velocities $v_{T_{\parallel,\perp}}$ are introduced in order to compare the dispersion/stability properties of these two models with the limit (ideal) case of a BM distribution function. Assuming the same temperature, the shape of the distribution function is only changed by the power indices $\kappa_{\parallel,\perp}$ and κ. Thus, in the limit of infinitely large power indices ($\kappa \to \infty$), both the PBK and the BK distribution functions converge to the same BM distribution function.

Both differences between and similarities of these two models have been discussed in Paper I, and more recently by Lazar et al. (2012b). In comparison with the additive BK model, where the distributions in the parallel and perpendicular directions are coupled and both are described by the same power index κ, the PBK model

is more flexible, modelling the gyrotropic VDFs with two distinct temperatures $T_\parallel \neq T_\perp$ and two independent power indices $\kappa_\parallel \neq \kappa_\perp$. Thus, the PBK can be more realistic in a turbulent plasma, where the mechanisms responsible for particle acceleration and formation of suprathermal tails (e.g. wave–particle interactions) are independent and distinct with respect to the direction of magnetic field, e.g. Landau damping accelerates particles parallel to $\boldsymbol{B}_0$, and cyclotron damping in the transverse direction. We also recall the prominent asymmetry of the PBK distribution (see contours in fig. 1 from Paper I) that suggests free energy in excess, and, possibly, an enhancement of the instability. These expectations have been confirmed for the Weibel instability (Lazar et al. 2010) and the whistler electron–cyclotron instability (Paper I).

3 DISPERSION FORMALISM

Electromagnetic waves propagating parallel to the uniform magnetic field are circularly polarized with right-hand (RH) and left-hand (LH) polarizations. Dispersion relations have been derived in Paper I, equation 8 for a PBK plasma, and equation 11 for a BK plasma. Here, we only consider LH modes, and for a PBK model the dispersion relation becomes (cf. Paper I)

$$k^2c^2 = \omega^2 + \sum_a \omega_{pa}^2 \left[\left(\frac{2\kappa_{a\parallel}+1}{2\kappa_{a\parallel}-1} \frac{T_{a\perp}}{T_{a\parallel}} - 1 \right) + \frac{2\kappa_{a\parallel}+1}{2\kappa_{a\parallel}(\kappa_{a\parallel}+1)} \frac{\Omega_a(\omega-\Omega_a)}{k^2\theta_{a\parallel}^2} + \left\{ \frac{2\kappa_{a\parallel}+1}{2\kappa_{a\parallel}-1} \frac{T_{a\perp}}{T_{a\parallel}} \frac{\omega-\Omega_a}{k\theta_{a\parallel}} + \frac{2\kappa_{a\parallel}+1}{2(\kappa_{a\parallel}+1)} \times \left[1 + \frac{(\omega-\Omega_a)^2}{\kappa_{a\parallel}k^2\theta_{a\parallel}^2} \right] \frac{\Omega_a}{k\theta_{a\parallel}} \right\} Z_{\kappa_\parallel}(f_1) \right], \quad (7)$$

with the dispersion function

$$Z_{\kappa_\parallel}(f) = \frac{1}{\pi^{1/2}\kappa_\parallel^{1/2}} \frac{\Gamma[\kappa_\parallel+2]}{\Gamma\left[\kappa_\parallel+3/2\right]} \times \int_{-\infty}^{+\infty} \mathrm{d}x \, \frac{(1+x^2/\kappa_\parallel)^{-\kappa_\parallel-2}}{x-f}, \quad \Im(f)>0, \quad (8)$$

of argument

$$f_a = \frac{\omega-\Omega_a}{k\theta_{a\parallel}}. \quad (9)$$

The parallel thermal velocity $\theta_{a\parallel}$ is defined in equation (2). For the same LH modes in a BK plasma, the dispersion relation reads

$$k^2c^2 = \omega^2 + \sum_a \omega_{pa}^2 \left\{ \left(\frac{T_{a\perp}}{T_{a\parallel}} - 1 \right) + \left[\frac{T_{a\perp}}{T_{a\parallel}} \frac{\omega-\Omega_a}{k\theta_{a\parallel}} + \frac{\Omega_a}{k\theta_{a\parallel}} \right] Z_\kappa^0(f_1) \right\}, \quad (10)$$

with the dispersion function (Lazar, Schlickeiser & Shukla 2008b)

$$Z_\kappa^0(f) = \frac{1}{\pi^{1/2}\kappa^{1/2}} \frac{\Gamma(\kappa)}{\Gamma\left(\kappa-\frac{1}{2}\right)} \times \int_{-\infty}^{\infty} \mathrm{d}x \, \frac{(1+x^2/\kappa)^{-\kappa}}{x-f}, \quad \Im(f)>0, \quad (11)$$

and the same argument in equation (9). But in this case, $\theta_{a\parallel}$ is given by equation (5). We keep the symbols introduced in Paper I for the plasma and wave parameters. The dispersion relations in equations (7) and (10) enable a general analysis for an arbitrary number of plasma species, and generalized power-law distributions, which include the more ideal cases of BM plasmas (in the limit of large $\kappa_\parallel$, $\kappa \to \infty$).

Because the electrons are non-resonant at EMIC scales, i.e. $|f_e| = |\omega - \Omega_e|/(k\theta_{e\parallel}) \gg 1$, their effects are negligible and we can consider isotropic ($A_e = 1$). Consequently, the dispersion relations (7) and (10) reduce, respectively, to

$$\frac{k^2c^2}{\omega_{p,p}^2} + \frac{\omega}{\Omega_p} = \frac{2\kappa_{p\parallel}+1}{2\kappa_{p\parallel}-1} A_p - 1 + \frac{2\kappa_{p\parallel}+1}{2\kappa_{p\parallel}(\kappa_{p\parallel}+1)} f_p\, g_p + \left[\frac{2\kappa_{p\parallel}+1}{2\kappa_{p\parallel}-1} A_p f_p + \frac{2\kappa_{p\parallel}+1}{2(\kappa_{p\parallel}+1)} \times \left(1 + \frac{f_p^2}{\kappa_{p\parallel}} \right) g_p \right] Z_{\kappa_\parallel}(f_p), \quad (12)$$

where $\theta_\parallel$ is given by equation (2), and

$$\frac{k^2c^2}{\omega_{p,p}^2} + \frac{\omega}{\Omega_p} = \left[A_p\, f_p + g_p \right] Z_\kappa^0(f_p) + A_p - 1, \quad (13)$$

where $\theta_\parallel$ is given by equation (5). For simplicity, we introduce $g_p = \Omega_p/(k\theta_{p\parallel})$.

4 THE INSTABILITY CONDITIONS

EMIC solutions are unstable only for those plasma parameters satisfying the instability condition, i.e. for sufficiently large temperature anisotropy, exceeding the instability threshold. Analytically, the unstable solutions can be described only in the limits of large ($|f_p| \gg 1$) or small ($|f_p| \ll 1$) arguments of the plasma dispersion function. For this reason, the instability condition, strictly depending on the plasma parameters and also covering the resonant regimes, i.e. $|f_p| \sim 1$, is obtained numerically.

The instability thresholds are derived for different levels of the maximum growth rates, viz. $\gamma_m/\Omega_p = 10^{-3}$, 10^{-2} and 10^{-1}. The lowest are relevant for the marginal (in)stability condition ($\gamma_m \to 0$). The anisotropy thresholds are calculated for an extensive range of the plasma beta parameter $0.01 \leq \beta_{p,\parallel} \leq 10$, including the solar wind and magnetospheric plasma conditions, and are fitted with an inverse correlation law (Gary & Lee 1994)

$$A_p = 1 + \frac{a}{\beta_{p,\parallel}^b}. \quad (14)$$

Values of the fitting parameters a and b are presented in Tables 1 and 2, and the corresponding contours of the maximum growth rates (in units of Ω_p) are displayed in Figs 1 and 2. We compare three models: the BM (solid lines), the less ideal PBK (dashed lines) and

Table 1. Proton temperature anisotropy fitting parameters from equation (14) for $\kappa = \kappa_\parallel = 2$.

	$\gamma = 10^{-1}\Omega_p$		$\gamma = 10^{-2}\Omega_p$		$\gamma = 10^{-3}\Omega_p$	
Model	a	b	a	b	a	b
BK	1.67	0.50	0.61	0.44	0.28	0.44
PBK	0.94	0.52	0.60	0.42	0.56	0.41
BM	1.33	0.48	0.64	0.41	0.45	0.40

Table 2. Proton temperature anisotropy fitting parameters from equation (14) for $\kappa = \kappa_{\parallel} = 6$.

	$\gamma = 10^{-1}\Omega_p$		$\gamma = 10^{-2}\Omega_p$		$\gamma = 10^{-3}\Omega_p$	
Model	a	b	a	b	a	b
BK	1.37	0.48	0.62	0.42	0.37	0.42
PBK	1.35	0.49	0.82	0.38	0.77	0.36
BM	1.33	0.48	0.64	0.41	0.45	0.40

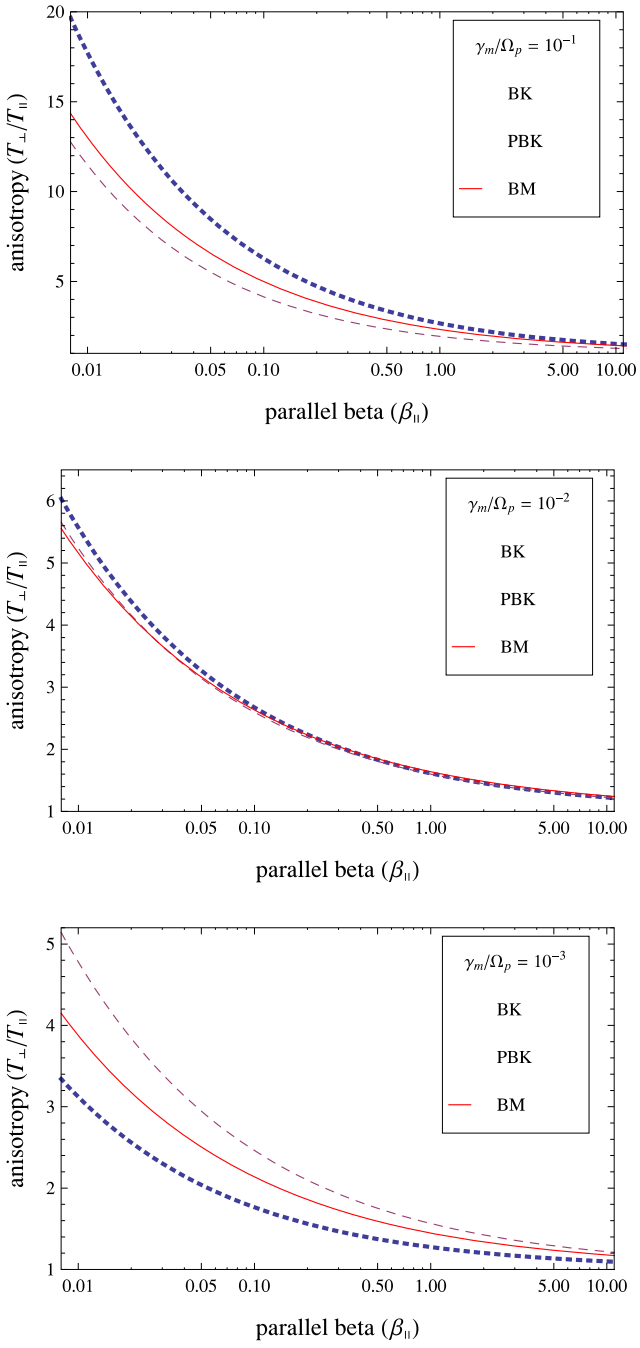

Figure 1. Thresholds of the EMIC instability for three levels of the maximum growth rates $\gamma_m/\Omega_p = 10^{-1}$ (top), 10^{-2} (middle) and 10^{-3} (bottom) as provided by three models: BK with $\kappa = 2$ (dotted lines), PBK with $\kappa_{\parallel} = 2$ (dashed lines), and BM with solid lines.

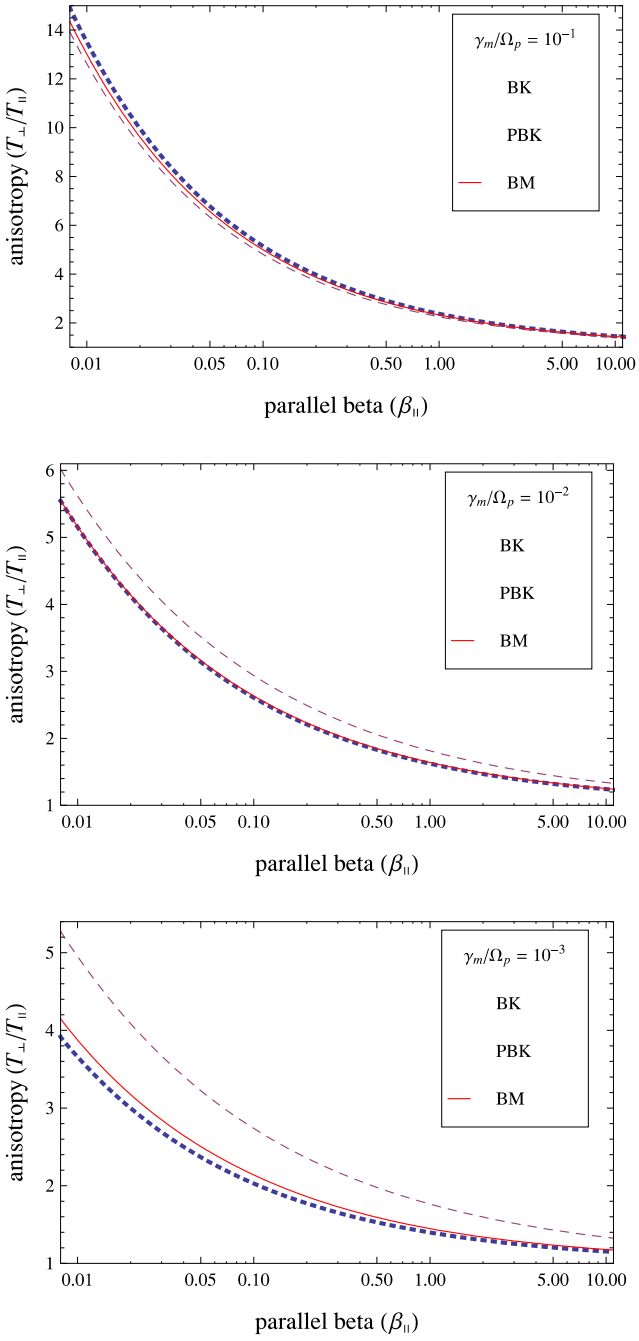

Figure 2. Thresholds of the EMIC instability for three levels of the maximum growth rates $\gamma_m/\Omega_p = 10^{-1}$ (top), 10^{-2} (middle) and 10^{-3} (bottom) as provided by three models: BK with $\kappa = 6$ (dotted lines), PBK with $\kappa_{\parallel} = 6$ (dashed lines) and BM with solid lines.

the BK (dotted lines) for $\kappa_{\parallel} = \kappa = 2$ in Fig. 1, and for $\kappa_{\parallel} = \kappa = 6$ in Fig. 2.

The anisotropy thresholds decrease with the increasing plasma beta parameter $\beta_{\parallel}$ because the instability is stimulated for higher values of the parallel temperature $T_{\parallel}$ or less intense magnetic fields B_0. For low values of the power index (Fig. 1), the relatively high growth rates $\gamma_m/\Omega_p = 10^{-1}$ are dominated by the PBK instability with the lowest thresholds. Moving down to lower levels of the growth rate ($\gamma_m/\Omega_p = 10^{-3}$), the PBK thresholds decrease and the BK thresholds become the lowest and the most relevant for marginal

(in)stability ($\gamma_m \to 0$). For higher values of the power index κ (Fig. 2), the evolution is almost the same, but with less contrast between the BK and BM thresholds (as also found in Paper I for the whistler instability).

Moreover, the effect of suprathermal populations is highly dependent on the threshold level (γ_m/Ω_p) and the power index, but not in the same way for the two Kappa models. These effects are highlighted by comparing the corresponding pair of panels from Figs 1 and 2. The instability is stimulated in the presence of suprathermals, lowering the thresholds with a decreasing power index for both Kappa models. This effect is significant only for the BK model, see the bottom panel in Fig. 1, while the PBK thresholds show an oscillatory evolution, which we correlate with the growth rates in the next section.

5 CORRELATING THRESHOLDS AND GROWTH RATES

Growth rates of the EMIC instability are derived numerically and are displayed in Figs 3–6 for two different plasma beta conditions, viz. $\beta_{p,\parallel} = 0.05$ and $\beta_{p,\parallel} = 1$. We compare the same models: the BM (solid lines) and the less ideal PBK (dashed lines) and BK (dotted lines) for $\kappa_\parallel = \kappa = 2$ in Figs 3 and 4, and for $\kappa_\parallel = \kappa = 6$ in Figs 5 and 6. Correlation can be made to the instability threshold conditions, if temperature anisotropies are chosen sufficiently low, in the range of their threshold values.

First, let us compare the unstable solutions provided by the two Kappa models. The discrepancy between these Kappa models becomes more important at large values of $\beta_\parallel$, but is diminished with the increasing power index κ, and both converge to the same Maxwellian solution for infinitely large $\kappa \to \infty$. For moderate values of the anisotropy, the instability is inhibited by the BK models, and it can be stimulated by the PBK distributions at sufficiently large wavenumbers. Also remark the wavenumber intervals in Figs 3 and 4, middle panels, where the PBK is stable and the BK (or BM) is unstable (lower wavenumbers), and vice versa (higher wavenumbers). If the anisotropy is not large enough, the low wavenumber solutions provided by the PBK model are highly damped.

For each of these two models, the effect of suprathermal protons on the growth rates is consistent with that found above for the thresholds, and can be evaluated by comparing the unstable solutions obtained for the same conditions and power indices. For instance, we compare Figs 3(b) and 5(b), or Figs 4(a) and 6(a), but also Figs 4(b) and 6(c), or Figs 4(d) and 6(d). The growth rates yielded by the BK model increase monotonically with increasing the power index κ. But those obtained from a PBK model behave oscillatory, first decreasing with $\kappa_\parallel$, to even lower values than those obtained for the BM model, and then increasing again, reaching the BM growth rates for a very large $\kappa_\parallel \to \infty$.

Now, if we allow the parameters to vary, we can evaluate the evolution of the unstable solutions with A and $\beta_\parallel$. Comparing to Fig. 3, maximum growth rates obtained in Fig. 4 increase faster with the temperature anisotropy. Higher growth rates are obtained for higher anisotropies and show a clear dominance of the PBK instability. This difference becomes less significant with a decreasing anisotropy, and the PBK plasmas reach the marginal stability before the BK and BM models. But this evolution is again markedly dependent on the plasma beta parameter and the power index, e.g. for higher values $\kappa = \kappa_\parallel = 6$ (Figs 5 and 6), these differences are less pronounced.

The influence of suprathermals on the oscillatory frequency of the EMIC instability is shown in Fig. 7. Remark that this effect

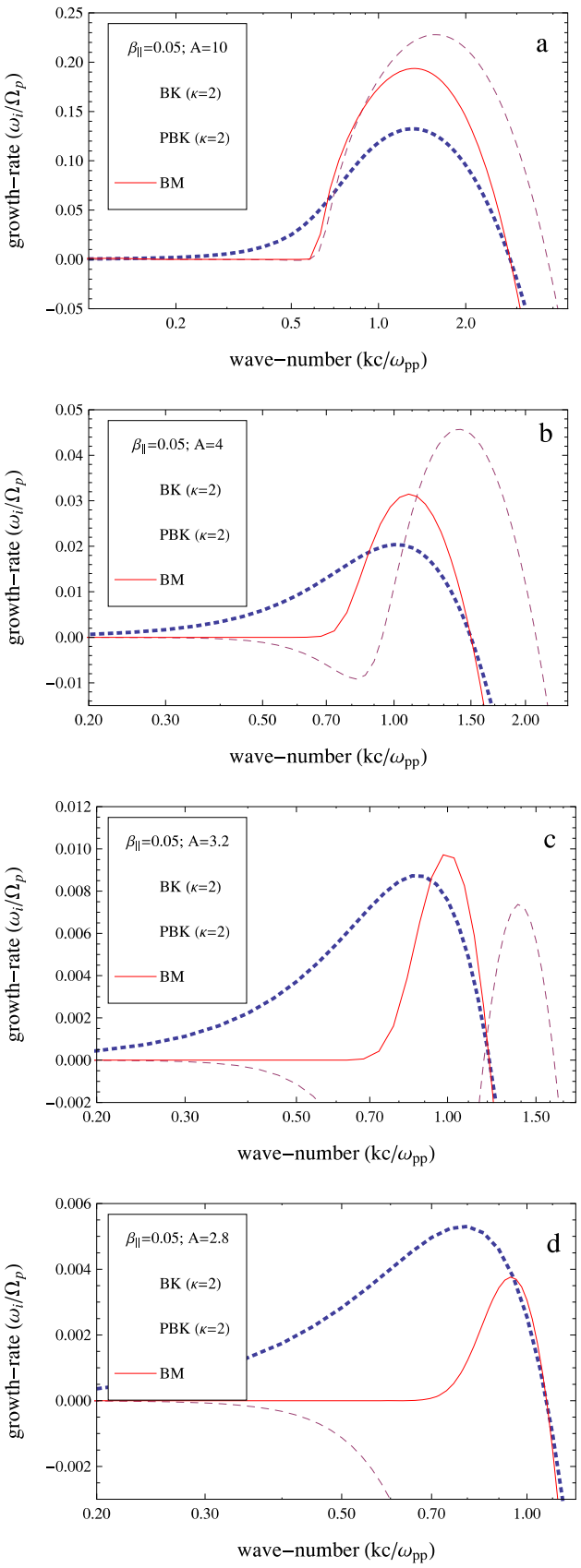

Figure 3. Growth rates of the EMIC instability as provided by three models: BK with $\kappa = 2$ (dotted lines), PBK with $\kappa_\parallel = 2$ (dashed lines) and BM (with solid lines) for $\beta_\parallel = 0.05$ and different temperature anisotropies.

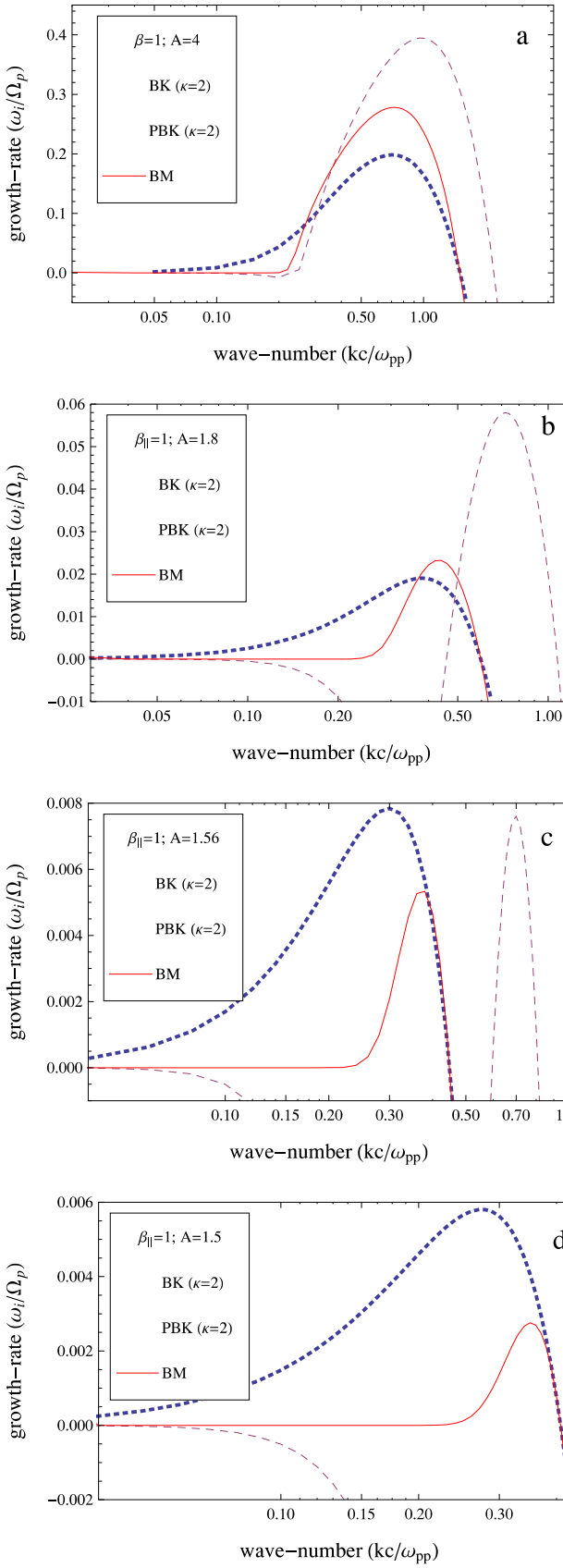

Figure 4. Growth rates of the EMIC instability as provided by three models: K with $\kappa = 2$ (dotted lines), PBK with $\kappa_{\|} = 2$ (dashed lines) and BM (with solid lines) for $\beta_{\|} = 1$ and different temperature anisotropies.

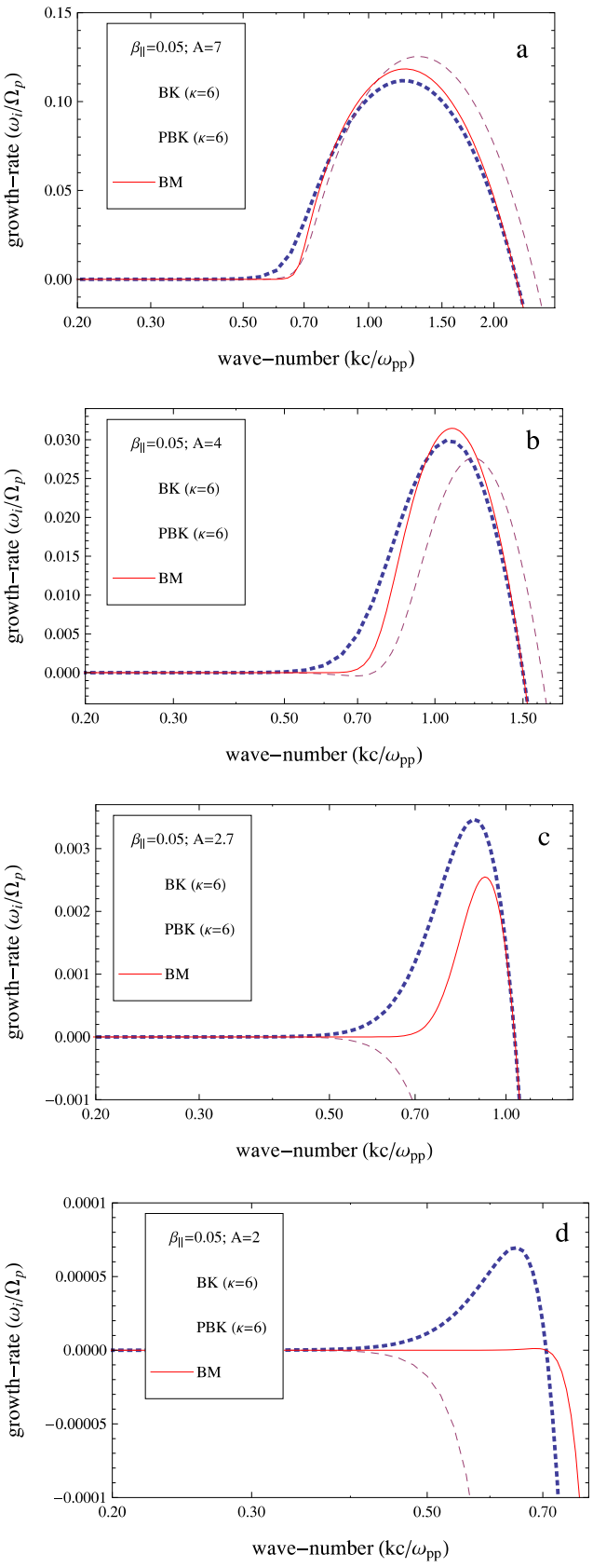

Figure 5. Growth rates of the EMIC instability as provided by three models: BK with $\kappa = 6$ (dotted lines), PBK with $\kappa_{\|} = 6$ (dashed lines), and BM (with solid lines) for $\beta_{\|} = 0.05$ and different temperature anisotropies.

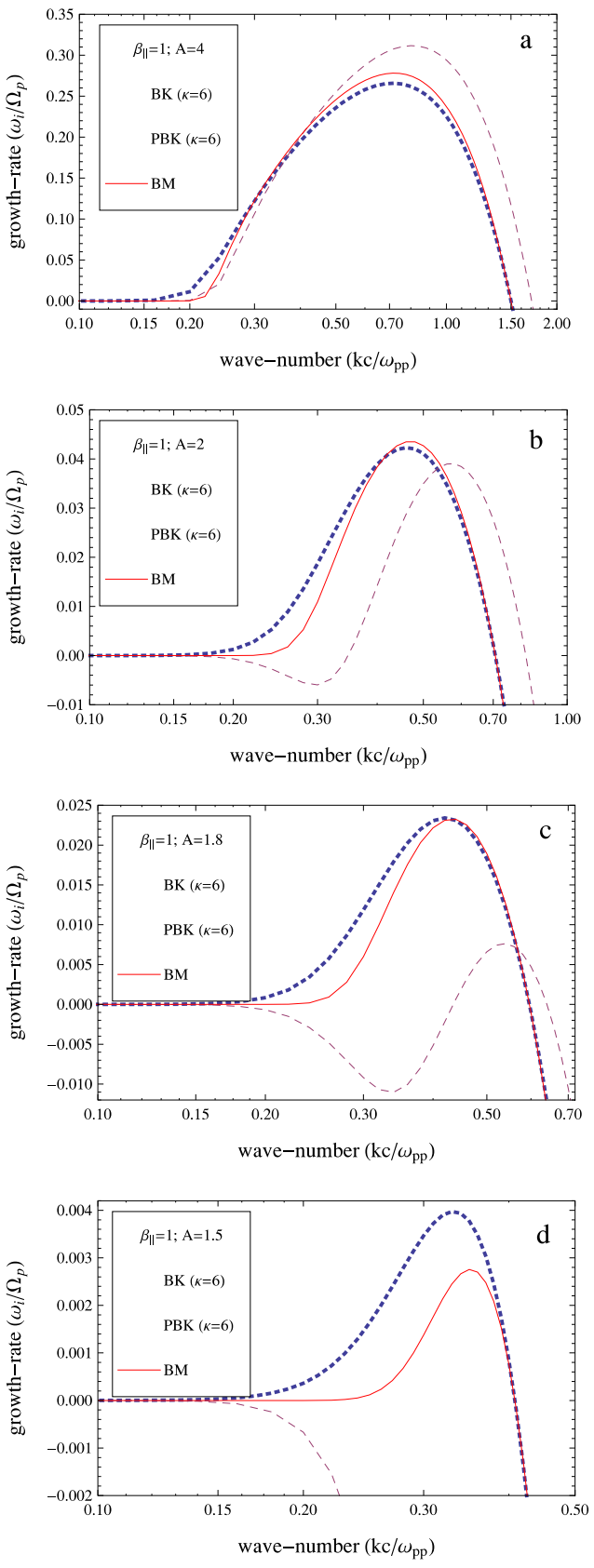

Figure 6. Growth rates of the EMIC instability as provided by three models: BK with $\kappa = 6$ (dotted lines), PBK with $\kappa_{\|} = 6$ (dashed lines), and BM (with solid lines) for $\beta_{\|} = 1$ and different temperature anisotropies.

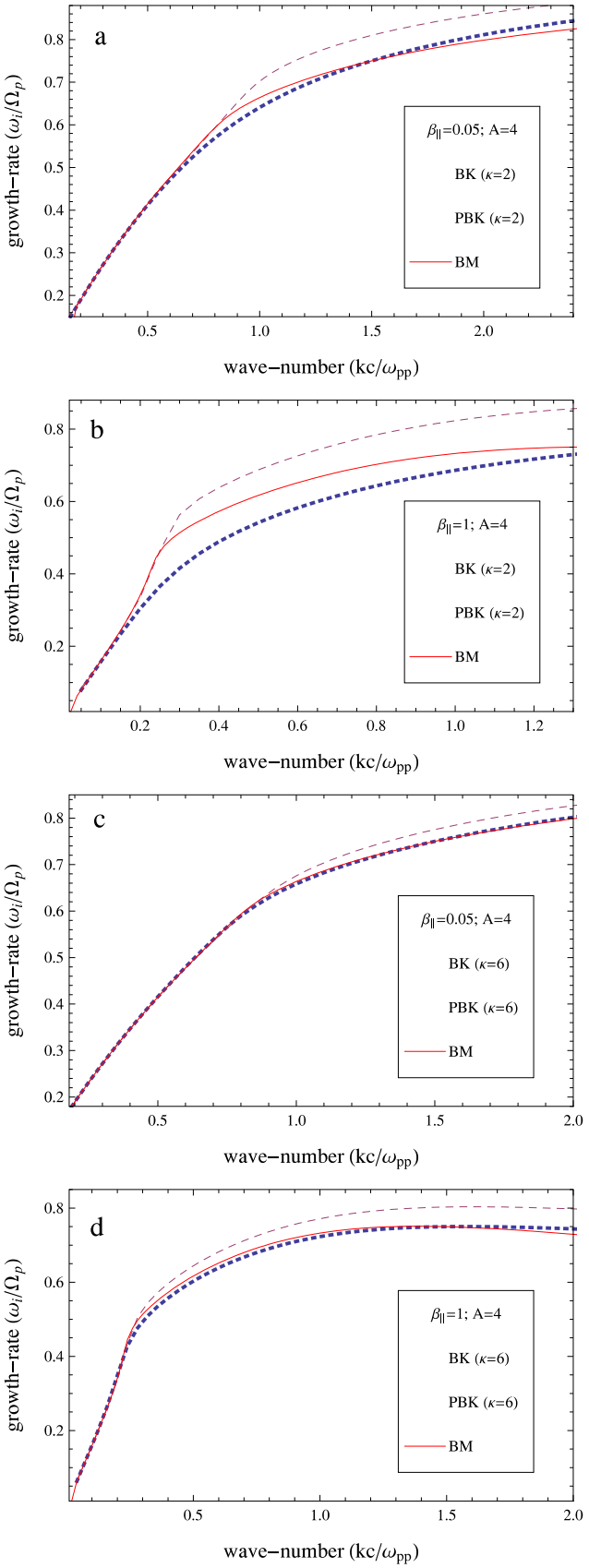

Figure 7. Frequency of the EMIC instability as provided by three models: BK with $\kappa = 2$ and 6 (dotted lines), PBK with $\kappa_{\|} = 2$ and 6 (dashed lines), and BM (solid lines) for $A = 4$ and two values of the plasma beta parameter.

can be significant for the PBK distributed plasmas, where the wave frequency is in general enhanced by comparison to a BM. The frequency uppershift is maximum for sufficiently large $\beta_{\parallel}$ and low power indices $\kappa = \kappa_{\parallel} \to 2$ (panel b in Fig. 7). For the same conditions, the wave frequency presents maximum downshifts in the BK model, which otherwise does not change significantly by comparison to the BM distributed plasmas.

6 CONCLUSIONS

One important driver of the EMIC instability is the excess of perpendicular temperature with respect to the direction of the local uniform magnetic field. In addition, the results obtained here clearly show that this instability is markedly sensitive to the shape of the anisotropic VDFs. This is based on a comparative analysis of the wave unstable solutions predicted by two Kappa models, namely the BK and PBK distribution functions, and the more standard BM model.

Previous studies have limited to compare the BK and BM models, showing that in the presence of suprathermal protons the instability is inhibited at large anisotropies, but can be stimulated at low anisotropies. In this case, the instability threshold is lowered by the suprathermals. Modelling suprathermals with the new PBK distribution function, here we find opposite effects: the instability is markedly stimulated at large anisotropies, but is inhibited at low anisotropies. The PBK distributed plasmas are less susceptible to the EMIC instability, because suprathermals strengthen the thresholds in this case.

Modelling the anisotropic populations observed in the solar wind and terrestrial magnetosphere with advanced power-law distribution functions should produce more realistic predictions on the role the EMIC instability can play in these environments. It is now the goal of the observational analysis to provide a double confirmation, whether these waves are stimulated or not by the suprathermal protons provided their temperature anisotropy is well modelled by the Kappa models in velocity space. For instance, the BK model can be associated with particle distributions in the slow winds from a quiet Sun, and with small deformations of the halo (Pilipp et al. 1987b; Marsch 2006, 2012). Instead, the PBK distribution function seems to be more appropriate to model VDFs in the fast solar wind with a prominent strahl component in the direction of magnetic field (Pilipp et al. 1987b; Lazar et al. 2012b). The double-strahl distributions observed at magnetic reconnection sites (Pilipp et al. 1987a; Gosling et al. 2005) are reproduced qualitatively well by a symmetric PBK model (Lazar et al. 2012b). The results presented here could therefore provide the first preliminary indications for a future refined analysis of this instability in space plasmas, and resolve disagreements between the observations and the less realistic dispersion models proposed before.

ACKNOWLEDGEMENTS

ML acknowledges financial support from the EU Commission and Research Foundation Flanders (FWO) as FWO Pegasus Marie Curie Fellow (grant 1.2.070.13). The authors acknowledge support from the Katholieke Universiteit Leuven. These results were obtained in the framework of the projects GOA/2009-009 (KU Leuven), G.0729.11 (FWO-Vlaanderen) and C 90347 (ESA Prodex 9). The research leading to these results has also received funding from the European Commission's Seventh Framework Programme (FP7/2007-2013) under the grant agreements SOLSPANET (project no. 269299, www.solspanet.eu), SPACECAST (project no. 262468, fp7-spacecast.eu), eHeroes (project n 284461, www.eheroes.eu) and SWIFF (project no. 263340, www.swiff.eu).

REFERENCES

Bale S. D., Kasper J. C., Howes G. G., Quataert E., Salem C., Sundkvist D., 2009, Phys. Rev. Lett., 103, 211101
Basu B., 2008, Phys. Plasmas, 15, 042108
Basu B., 2009, Phys. Plasmas, 16, 052106
Basu B., Grossbard N. J., 2011, Phys. Plasmas, 18, 092106
Cattaert T., Hellberg M., Mace R., 2007, Phys. Plasmas, 14, 082111
Christon S. P., Williams D. J., Mitchell D. G., Huang C. Y., Frank L. A., 1991, J. Geophys. Res., 96, 1
Collier M. R., Hamilton D. C., Gloeckler G., Bochsler P., Sheldon R. B., 1996, Geophys. Res. Lett., 23, 1191
Fisk L. A., Gloeckler G., 2006, ApJ, 640, L79
Gary S. P., Lee M. A., 1994, J. Geophys. Res., 99, 11,297
Gary S. P., Skoug R. S., Steinberg J. T., Smith C. W., 2001, Geophys. Res. Lett., 28, 2759
Gosling J. T., Skoug R. M., McComas D. J., Smith C. W., 2005, J. Geophys. Res., 110, A01107
Hellberg M., Mace R., 2002, Phys. Plasmas, 9, 1495
Hellberg M., Mace R., Cattaert T., 2005, Space Sci. Rev., 121, 127
Isenberg P. A., 2001, Space Sci. Rev., 95, 119
Jian L. K., Russell C. T., Luhmann J. G., Strangeway R. J., Leisner J. S., Galvin A. B., 2009, ApJ, 701, L105
Kennel C. F., Petschek H. E., 1966, J. Geophys. Res., 71, 1
Lazar M., Schlickeiser R., Shukla P. K., 2008b, Phys. Plasmas, 15, 042103
Lazar M., Schlickeiser R., Poedts S., 2010, Phys. Plasmas, 17, 062112
Lazar M., Poedts S., Schlickeiser R., 2011, MNRAS, 410, 663 (Paper I)
Lazar M., Schlickeiser R., Poedts S., 2012a, in Lazar M., ed., Exploring the Solar Wind. InTech, Rijeka, p. 241, available at: http://www.intechopen.com/books/exploring-the-solar-wind/
Lazar M., Pierrard V., Poedts S., Schlickeiser R., 2012b, Astrophys. Space Sci., 33, 97
Maksimovic M., Pierrard V., Riley P., 1997, Geophys. Res. Lett., 24, 1151
Maksimovic M. et al., 2005, J. Geophys. Res., 24, A09104
Marsch E., 2006, Living Rev. Solar Phys., 3, 1
Marsch E., 2012, Space Sci. Rev., 172, 23
Matteini L., Landi S., Hellinger P., Pantellini F., Maksimovic M., Velli M., Goldstein B. E., Marsch E., 2007, Geophys. Res. Lett., 34, L20105
Nguyen S. T., Perez J. D., Fennell J. F., 2007, J. Geophys. Res., 112, A12203
Pierrard V., Lazar M., 2010, Sol. Phys., 267, 153
Pierrard V., Maksimovic M., Lemaire J., 1999, J. Geophys. Res., 104, 17021
Pilipp W. G., Miggenrieder H., Montgomery M. D., Muehlhaeuser K.-H., Rosenbauer H., Schwenn R., 1987a, J. Geophys. Res., 92, 1093
Pilipp W. G., Miggenrieder H., Muehlhaeuser K.-H., Rosenbauer H., Schwenn R., Neubauer F. M., 1987b, J. Geophys. Res., 92, 1103
Summers D., Thorne R. M., 1991, Phys. Fluids B, 3, 1835
Thomsen M. F., Gary S. P., Feldman W. C., Cole T. E., Barr H. C., 1983, J. Geophys. Res., 88, 3035
Tsallis C., 1995, Physica A, 221, 277
Vasyliunas V. M., 1968, J. Geophys. Res., 73, 2839
Xue S., Thorne R. M., Summers D., 1993, J. Geophys. Res., 98, 17475
Xue S., Thorne R. M., Summers D., 1996a, J. Geophys. Res., 101, 15457
Xue S., Thorne R. M., Summers D., 1996b, J. Geophys. Res., 101, 15467

This paper has been typeset from a TEX/LATEX file prepared by the author.